Quantum states in a champagne bottle

1998 J. Phys. A: Math. Gen. 31 657

(http://iopscience.iop.org/0305-4470/31/2/022)

J. Phys. A: Math. Gen. **31** (1998) 657–670. Printed in the UK PII: S0305-4470(98)86984-9

Quantum states in a champagne bottle

M S Child

Physical and Theoretical Chemistry Laboratory, Oxford OX1 3QZ, UK

Received 20 August 1997

Abstract. Features of the classical mechanics under the potential $V = -a(X^2+Y^2)+b(X^2+Y^2)^2$ are related to the quantum-mechanical spectrum. A known topological obstruction to the existence of global action-angle variables is shown to be reflected in a sharp change in the disposition of eigenvalues around $E = 0$. The energies of states labelled by a radial quantum number v vary smoothly with the angular momentum ℓ for $E < 0$ but have a discontinuous derivative at $\ell = 0$ for $E > 0$. An alternative labelling $|n, \ell\rangle$, where $n = 2v + |\ell|$ shows the opposite effect. Semiclassical arguments based on the forms of positive and negative energy trajectories also suggest a near symmetry between the positive second derivative $(\partial^2 E/\partial \ell^2)_v$ at energy $-\epsilon$ and the negative counterpart $(\partial^2 E/\partial \ell^2)_n$ at energy ϵ, which is confirmed in the quantum-mechanical spectrum. Minor deficiencies in the Bohr–Sommerfeld rule are removed by introducing an analytical phase correction $\eta(\epsilon, \ell)$ for states with $\epsilon \simeq 0$ and $\ell \simeq 0$.

1. Introduction

Connections between the classical and quantum mechanics of linear motion in a symmetric double-well potential are well established [1]. The purpose of this paper is to explore similar connections for the planar analogue, with added angular momentum around the figure axis, which has been brought into prominence by Bates [2] from whom the title of the paper has been borrowed. The point of interest is that the champagne bottle is the simplest member of a class of systems for which the classical mechanics is complicated by a common gross topological obstruction to the global construction of angle-action variables; others include the spherical pendulum [3, 4], the Lagrange top [5] and the Hamiltonian Hopf bifurcation [6]. Questions as to the possible influence of this classical obstruction on the quantum-mechanical spectrum are relevant to the wide amplitude bending plus skipping rotational motions of a bent molecule, which are now on the verge of being experimentally observable. Aspects of this bent/linear transition have been addressed in the molecular physics literature [7] in the context of constructing a computationally tractable Hamiltonian, but the global nature of the quantum-mechanical spectrum has not previously been considered.

The topological obstruction arises from the presence of a fixed point at the crown of the bulge in the bottle, which is conveniently taken as the energy zero; it divides the energy surface into topological types $S^2 \times S^1$ for $E < 0$ and S^3 for $E > 0$ [2]. The classical motions lie on two types of torus and a computation of the monodromy of the torus bundle demonstrates the absence of any smooth connection between the two types. The connection with quantum mechanics is obtained by labelling the tori at different energies, E, and angular momenta, L, by actions (I_θ, I_R), in which case the monodromy is seen to be associated with a discontinuity in the partial derivative $(\partial I_R/\partial L)_E$ at $L = 0$ for $E > 0$ but not for $E < 0$, which is a symptom of the discontinuity between the two types of torus.

0305-4470/98/020657+14$19.50

An alternative labelling with actions (I_θ, I_N) where $I_N = 2I_R + |I_\theta|$ is shown below to transfer the discontinuity (now in $(\partial I_N/\partial L)_E$ at $L = 0$) to $E < 0$, from which it is argued that the tori at negative and positive energies have valid local actions (I_θ, I_R) and (I_θ, I_N) respectively.

The influence on the quantum-mechanical spectrum follows from the substitution $I_\theta = \ell h$, $I_R = (v + \frac{1}{2})h$ and $I_N = (n + 1)h$, coupled with the identities $(\partial E/\partial \ell)_v = -h(\partial I_R/\partial L)_E/(\partial I_R/\partial E)_L$ and $(\partial E/\partial \ell)_n = -h(\partial I_N/\partial L)_E/(\partial I_N/\partial E)_L$ and the observation that $(\partial I_R/\partial E)_L = (\partial I_N/\partial E)_L$, both being positive and continuous on the line $L = 0$ except at $E = 0$ for all (L, E). It follows that curves drawn through eigenvalues labelled by v, the number of radial nodes, will be continuously differentiable (with zero $(\partial E/\partial \ell)_v$ at $\ell = 0$ due to the symmetry in $\pm\ell$) for $E < 0$, but not for $E > 0$. The converse will apply for curves labelled by common values of $n = 2v + |\ell|$. An interesting near symmetry between the second derivatives $(\partial E^2/\partial \ell^2)_v$ for $E < 0$ and $(\partial E^2/\partial \ell^2)_n$ for $E > 0$ is also identified. These conclusions rest on the validity of the Bohr–Sommerfeld quantization rules. Comparison with numerically accurate quantum-mechanical computations reveals a systematic discrepancy for energy levels close to $E = 0$ and $\ell = 0$, which is removed by introducing an analytical phase correction $\eta(\epsilon, \ell)$, where ϵ is a reduced energy, the form of which is derived by making a comparison between the JWKB wavefunction [1] and the asymptotic form a Kummer function [8] that takes proper account of the singularity at $r = 0$.

2. Classical background

The Hamiltonian under consideration

$$H = \frac{1}{2m}(P_R^2 + P_\theta^2/R^2) - aR^2 + bR^4 \tag{1}$$

with $a > 0$ and $b > 0$, is cyclic in the polar angle θ; hence P_θ is conserved. The critical points include an unstable fixed point at the origin $R = 0$, $P_R = 0$ if $P_\theta = 0$ and rings of relative equilibria, with $P_R = 0$, whose radii depend on P_θ according to

$$\frac{P_\theta^2}{2m} + aZ^2 - 2bZ^3 = 0 \tag{2}$$

where $Z = R^2$. Equation (2) admits one real positive solution for each value of P_θ.

The Hamiltonian system is completely integrable because the energy and angular momentum are conserved. However, Bates [2] concludes on topological grounds that there can be no global angle-action variables because the energy surface is of topological type $S^2 \times S^1$ at negative energies, but of type S^3 when the energy is positive. The motions therefore lie on two types of tori, whose coordinate projections are illustrated in figure 1.

Further insight, along the lines suggested by Cushman and Duistermaat [3] and Bates [2], is obtained by defining action variables

$$\begin{aligned} I_\theta^\pm &= \oint P_\theta \, \mathrm{d}\theta = 2\pi L \\ I_R^\pm &= \oint P_R \, \mathrm{d}R = 2\int_{R_{\min}}^{R_{\max}} P_R \, \mathrm{d}R \end{aligned} \tag{3}$$

where

$$P_R = [2m(E + aR^2 - bR^4 - L^2/2mR^2)]^{\frac{1}{2}} \tag{4}$$

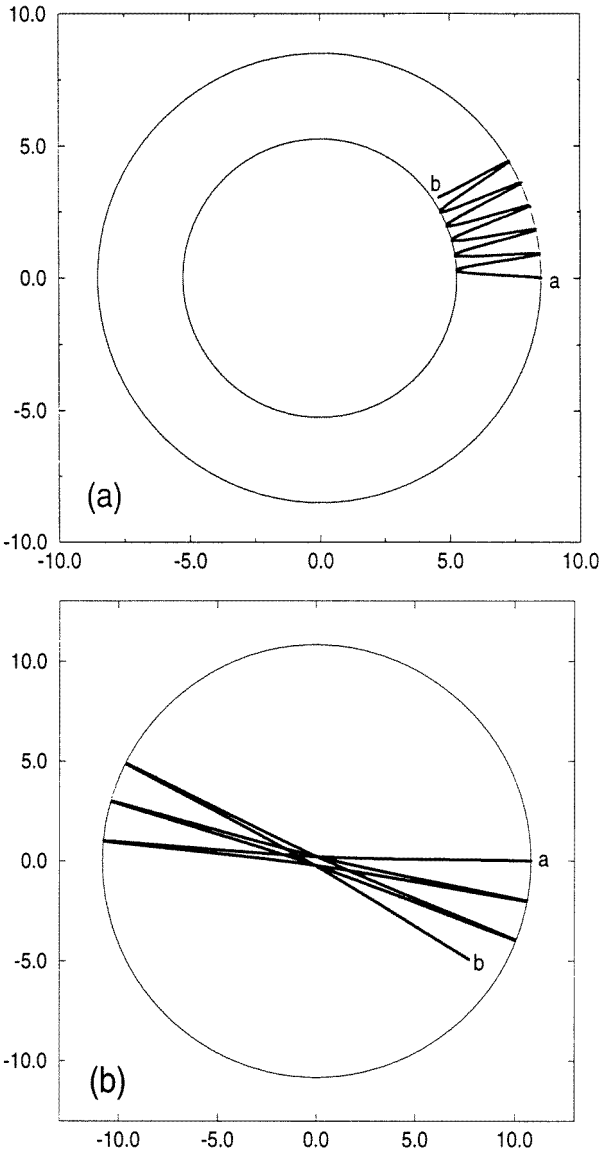

Figure 1. Trajectories with energies (*a*) $\epsilon = -10$ and (*b*) $\epsilon = +10$ for the scaled model with $m = 1$, $a = 0.5$, $b = 0.005$ and $|L| = 1$. Each trajectory is run for 25 time units with $L > 0$ (or $L < 0$) if it is taken to start at a (or b).

in which E is the energy, $R_{\min}$ and $R_{\max}$ are the radial turning points (at which $P_R = 0$) and $L = P_\theta$. The $+$ and $-$ refer to division of the set S of L values into subsets S_+ and S_- where

$$S_+ = S \cap \{L > 0\} \qquad S_- = S \cap \{L < 0\} \tag{5}$$

thus $I^+ = (I_\theta^+, I_R^+)$ are actions on S_+ and $I^- = (I_\theta^-, I_R^-)$ are actions on S_-.

There is no problem in assigning such actions to any given torus and the positions of those with regularly spaced (I_θ, I_R) are shown in figure 2 in the space defined by L and

E. The difficulties arise in passing smoothly from torus to another on a path γ around the origin. The following argument given by Bates [2], applies a geometrical construction due to Cushman and Duistermaat [3], to compute what is called the monodromy of the torus bundle. The holonomy involves parallel transport of a vector $\boldsymbol{\delta I} = (\delta I_\theta, \delta I_R)^T$ in regions S_+ and S_- coupled with parallel transport of the tangent vector $\boldsymbol{\delta J} = (\delta L, \delta E)^T$ across their junction at $L = 0$, where derivatives in the tangent relations

$$\delta \boldsymbol{I}^\pm = DI^\pm \delta \boldsymbol{J} \tag{6}$$

may be discontinuous. To show the origin of such discontinuities, Bates [2] noted that

$$\begin{aligned} DI^\pm &= \begin{pmatrix} (\partial I_\theta^\pm/\partial L) & (\partial I_\theta^\pm/\partial E) \\ (\partial I_R^\pm/\partial L) & (\partial I_R^\pm/\partial E) \end{pmatrix} \\ &= \begin{pmatrix} 2\pi, & 0 \\ A^\pm, & B^\pm \end{pmatrix} \end{aligned} \tag{7}$$

where

$$\begin{aligned} A^\pm &= -2L^\pm \int_{R_{\min}}^{R_{\max}} R^{-2} P_R^{-1}\, \mathrm{d}R \\ B^\pm &= 2m \int_{R_{\min}}^{R_{\max}} P_R^{-1}\, \mathrm{d}R \end{aligned} \tag{8}$$

with the understanding that $A^\pm$ and $B^\pm$ at points a and b on the path γ in figure 2 are evaluated by taking the limit $L \to 0$. It follows that $A_a^- = -A_a^+$, $A_b^- = -A_b^+$, $B_a^- = B_a^+$ and $B_b^- = B_b^+$. Note also that $A^\pm$ may be evaluated as [2]

$$A^\pm = -2 \int_{R_{\min}}^{R_{\max}} \frac{(\mathrm{d}\theta/\mathrm{d}t)}{(\mathrm{d}R/\mathrm{d}t)}\, \mathrm{d}R \tag{9}$$

which is just minus the increase of the polar variable θ when the radial motion completes one period. Reference to figures 1(a) and (b) respectively therefore shows that $A_a^\pm = 0$ in the limit $L \to 0$, with $E < 0$ while $A_b^\pm = \mp\pi$ when $E > 0$. It follows that the derivative $(\partial I_R/\partial L)$ is continuous at the point a, but discontinuous at the point b in figure 2.

To see the consequences for the monodromy, consider the initial vector $\boldsymbol{\delta I}_a^+$ originating at a in S_+ in figure 2(b), which joins points with I_θ values that differ by five units (because only every fifth L value is shown) and with a common I_R value (in this case the seventh point from the bottom of each vertical column). In other words, $\boldsymbol{\delta I}_a^+ = (5, 0)^T$. Parallel transport of $\boldsymbol{\delta I}_a^+$ within S_+ generates the other vectors $\boldsymbol{\delta I}^+$ with the same action differences, but the lengths and orientations of the tangent vector $\boldsymbol{\delta J}^+$ indicated by the solid arrows vary according to the inverse of equation (6). On reaching the point b, $\boldsymbol{\delta I}_b^+$ is taken across $L = 0$ by parallel transport of $\boldsymbol{\delta J}$ to produce the broken arrow that terminates at b in figure 2(b). In other words, using equation (6) and its inverse.

$$\boldsymbol{\delta I}_b^- = DI_b^-(DI_b^+)^{-1}\boldsymbol{\delta I}_b^+ = DI_b^-(DI_b^+)^{-1}\boldsymbol{\delta I}_a^+. \tag{10}$$

The second half of the cycle is completed in the same way. The final result, after recrossing $L = 0$ at a, shows that the initial and final vectors, $\boldsymbol{\delta I}_a^+$ and $(\boldsymbol{\delta I}_a^+)'$ respectively are related by

$$(\boldsymbol{\delta I}_a^+)' = M(\boldsymbol{\delta I}_a^+) \tag{11}$$

where the monodromy is given by

$$M = DI_a^+(DI_a^-)^{-1}DI_b^-(DI_b^+)^{-1}. \tag{12}$$

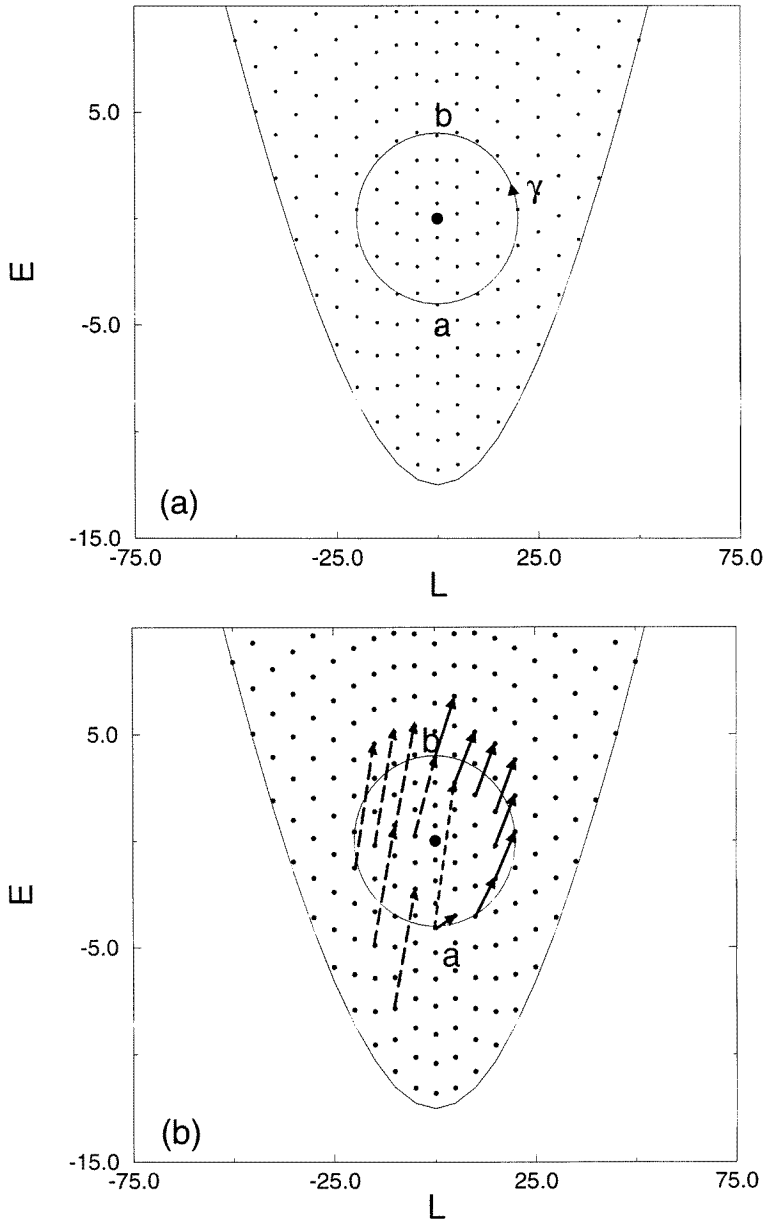

Figure 2. (*a*) The joint (L, E) spectrum on a uniform action grid with spacing $\Delta(I_\theta/\hbar) = 5$, $\Delta(I_\theta/h) = 1$, using the parameter values employed for figure 1. (*b*) Parallel transport around the path γ, according to the holonomy defined by equations (6) and (10). Broken arrows are employed after crossing the line $L = 0$.

The computation is completed by combining equation (7) with the symmetry relations $B_a^- = B_a^+$, $B_b^- = B_b^-$ and the values $A_a^\pm = 0$, $A_b^\pm = \mp\pi$ given above;

$$M = \begin{pmatrix} 1 & 0 \\ \frac{1}{\pi}(A_a^\pm - A_b^\pm) & 0 \end{pmatrix} = \begin{pmatrix} 1 & 0 \\ 1 & 1 \end{pmatrix}. \tag{13}$$

The conclusion is that the actions $I = (I_\theta, I_R)$ cannot be globally valid because transport of an arbitary vector $\boldsymbol{\delta I}_a^+$ around the cycle γ does not bring it back to itself—a problem that arises from the discontinuity in $(\partial I_R/\partial L)$ at $L = 0$ for $E > 0$.

No such discontinuity exists for $E < 0$, however, because $A_a^+ = A_a^- = 0$. Hence (I_θ, I_R) may be taken to be locally valid for $E < 0$ where both actions are continuously differentiable with respect to L and E. The question arises as to whether some combination of (I_θ, I_R) is locally valid in a similar sense for $E > 0$. The answer is suggested by the nature of the trajectory in figure 1(*b*), which is seen to pass through approximately two cycles of the radial motion for each cycle of θ. Thus, as in the angle-action theory of the degenerate harmonic oscillator [1, 9], it is natural to define a new total action

$$\begin{aligned} I_N^\pm &= 2I_R^\pm + |I_\theta^\pm| \\ &= 2I_R^\pm \pm 2\pi L^\pm \end{aligned} \tag{14}$$

such that

$$(\partial I_N^\pm/\partial L^\pm) = 2(A^\pm \pm \pi). \tag{15}$$

The additional terms $\pm\pi$ transfer the discontinuity from the points with $L = 0$, $E > 0$, where $A^\pm = \mp\pi$ to points with $L = 0$, $E < 0$, where $A^\pm = 0$. The new action I_N is therefore locally valid for $E > 0$ in the sense that applies to I_R for $E < 0$.

One should also note a consequence for the angle variables associated with the two sets of actions. In the (I_θ, I_R) system these are the polar angle θ and a radial angle θ_R that increases by 2π for each cycle of the radial motion. The appropriate canonical transformation [12] shows that the corresponding quantities in the (I_θ, I_N) system are $\theta' = \theta - \frac{1}{2}\theta_R$ and $\theta_N = \frac{1}{2}\theta_R$. The significance of the difference between θ and θ' is illustrated in figure 1; θ and θ' are in fact the proper precessional angles for the $\epsilon < 0$ and $\epsilon > 0$ trajectories respectively, and θ is seen to precess forward for $\ell > 0$, while θ' precesses backwards. The explanation, as discussed in the following section, is that the θ changes accompanying say two cycles of the radial motion for the two types of trajectory are related by $\Delta\theta_+ + \Delta\theta_- = 2\pi$ if $\epsilon_+ = -\epsilon_- > 0$, whereas θ_R increases by 4π. Thus $\Delta\theta'_+ = \Delta\theta_+ - 2\pi = -\Delta\theta_-$.

3. Bohr–Sommerfeld quantization

The nature of the spectrum in the semiclassical limit is determined by the Bohr–Sommerfeld quantization rules

$$\begin{aligned} I_\theta &= 2\pi P_\theta = \ell h \\ I_R &= (v + \tfrac{1}{2})h \end{aligned}$$

or

$$I_N = 2I_R + |I_\theta| = (2v + |\ell| + 1)h = (n + 1)h. \tag{16}$$

The labels $|v, \ell\rangle$ and $|n, \ell\rangle$ give alternative equivalent designations for any individual state, but if ℓ, v and n are treated as continuous variables it follows from the previous discussion that the derivatives $(\partial E/\partial \ell)_v$ and $(\partial E/\partial \ell)_n$ will differ. Thus $(\partial E/\partial \ell)_v = -(\partial v/\partial \ell)_v/(\partial v/\partial E)_\ell$ vanishes at $\ell = 0$ for $E < 0$ but not for $E > 0$, while the converse is true for $(\partial E/\partial \ell)_n = -(\partial n/\partial \ell)_v/(\partial n/\partial E)_\ell$.

To obtain quantitative results it is convenient to apply the scaling substitutions.

$$R = (\hbar^2/2ma)^{\frac{1}{4}} r \qquad E = (2a\hbar^2/m)\epsilon \qquad b = (8ma^3/\hbar^2)^{\frac{1}{4}}\beta \tag{17}$$

so that the quantization condition may be expressed as

$$(I_R/2\hbar) = \int_{r_{\min}}^{r_{\max}} \sqrt{2\epsilon + r^2 - 2\beta r^4 - \ell^2/r^2}\,\mathrm{d}r$$
$$= \frac{1}{2}\int_{z_{\min}}^{z_{\max}} \sqrt{\frac{2\epsilon z + z^2 - 2\beta z^3 - \ell^2}{Z}}\,\mathrm{d}z = \left(v + \frac{1}{2}\right)\pi \tag{18}$$

where $z = r^2$. Numerical determination of the energy levels therefore simply requires quadrature for the integral with adjustments to the energy until equation (18) is satisfied.

Relatively simple analytical results for $\ell = 0$, which include evidence of an approximate symmetry between the positive and negative energy spectra, are also available. The formulae differ according to the ordering of the two lowest roots of the cubic term in equation (18), which lie at

$$z = 0, (1 \pm \sqrt{1 + (\epsilon/\epsilon_0)})/4\beta \tag{19}$$

where ϵ_0 is the depth of the potential minimum, $V_{\min} = -\epsilon_0 = -(1/16\beta)$. At negative energies equation (18) yields, for $\ell = 0$

$$(v + \tfrac{1}{2}) = (8\epsilon_0/3\pi)(2 - k_-^2)^{3/2}[(2 - k_-^2)E(k_-) - 2(1 - k_-^2)K(k_-)] \tag{20}$$

where

$$k_-^2 = 2\sqrt{1 + (\epsilon/\epsilon_0)}/[[1 + \sqrt{1 + (\epsilon/\epsilon_0)}]] \tag{21}$$

and $E(k_-)$ and $K(k_-)$ are elliptic integrals [10, 11]. The corresponding forms at positive energies are

$$(v + \tfrac{1}{2}) = (8\epsilon_0/3\pi)(2k_+^2 - 1)^{3/2}[(2k_+^2 - 1)E(k_+) + (1 - k_+^2)K(k_+)] \tag{22}$$

and

$$k_+^2 = [1 + \sqrt{1 + (\epsilon/\epsilon_0)}]/2\sqrt{1 + (\epsilon/\epsilon_0)}]. \tag{23}$$

Equations (21) and (23) show that k_- varies between 0 and 1 over the energy range $-\epsilon_0 \leqslant \epsilon \leqslant 0$ while k_+^2 decreases from unity at $\epsilon = 0$ to 0.8536 at $\epsilon = \epsilon_0$ and 0.5 as $\epsilon \to \infty$. Insertion of the limiting values $E(0) = K(0) = \pi/2$, and $E(1) = \pi/2$ and $(1 - k^2)K(k) \to 0$ as $k \to 1$ [10] in equation (20) shows, as expected, that $v = -\frac{1}{2}$ at $\epsilon = -\epsilon_0$, while the number of negative energy states is given by the simple formula

$$v + \tfrac{1}{2} = (8\epsilon_0/3\pi) \tag{24}$$

at $\epsilon = 0$. In addition, equation (22) shows that $(v + \frac{1}{2})$ increases by a further $0.95(8\epsilon_0/3\pi)$ as ϵ increases to ϵ_0, which is one of the approximate symmetries of the system. Finally, it follows by expansion of the elliptic integrals in equation (20) to order k_-^4 [10] that

$$\epsilon \doteq -\epsilon_0 + \sqrt{2}(v + \tfrac{1}{2}) \tag{25}$$

for the lowest energy states.

A second approximate symmetry relates the record derivatives $(\partial^2\epsilon/\partial\ell^2)_v$ at $\ell = 0$ and $\epsilon < 0$ to $(\partial^2\epsilon/\partial\ell^2)_n$ at $\ell = 0$ and $\epsilon > 0$. Since the quantum numbers v and $n = 2v + |\ell|$ were chosen to ensure that the corresponding first derivatives would vanish, the second derivatives may be evaluated as

$$(\partial^2\epsilon/\partial\ell^2)_v = -(\partial^2 v/\partial\ell^2)_\epsilon/(\partial v/\partial\epsilon)_\ell \tag{26}$$

and similarly for $(\partial^2\epsilon/\partial\ell^2)_n$. The derivations start in both cases from the following derivative relations implied by equation (18) [10, 11]

$$\left(\frac{\partial v}{\partial \epsilon}\right)_\ell = \frac{1}{\pi}\frac{1}{\sqrt{2\beta(a-c)}}K(k)$$
$$\left(\frac{\partial v}{\partial \ell^2}\right)_\epsilon = -\frac{1}{2\pi}\frac{1}{\sqrt{2\beta(a-c)}}\Pi(\rho,k) \tag{27}$$

where

$$\rho = -\left(\frac{a-b}{a}\right)$$
$$k^2 = \left(\frac{a-b}{a-c}\right). \tag{28}$$

a, b and c are the roots given in equation (19) in the order $a > b > c$ and $\Pi(\rho, k)$ is an elliptic integral of the third kind [10, 11]. The case $\epsilon < 0$ is straightforward because $c = 0$ from which $\rho = -k^2$ and the known properties of $\Pi(-k^2, k)$ [11] yield

$$\left(\frac{\partial^2\epsilon}{\partial\ell^2}\right)_v = 2\beta\left(\frac{2-k_-^2}{1-k_-^2}\right)\frac{E(k_-)}{K(k_-)} \tag{29}$$

where k_- is given by equation (21). The case $\epsilon > 0$ is more complicated because $b \to 0$ as $\ell \to 0$; hence $\rho \to -1$ which leads to a divergence of $\Pi(\rho, k)$ [11], associated with the discontinuous first derivative $(\partial v/\partial\ell)\epsilon$ for $\epsilon > 0$. Replacing v by n in equations (27) leads to a cancellation of divergence from the term in $|l|$ on the left-hand side, and one finally obtains

$$\left(\frac{\partial^2\epsilon}{\partial\ell^2}\right)_n = -2\beta\left(\frac{2k_+^2-1}{1-k_+^2}\right)\frac{E(k_+)-(1-k_+^2)K(k_+)}{k_+^2K(k_+)} \tag{30}$$

where k_+ is given by equation (23).

It follows from (29) that $(\partial^2\epsilon/\partial\ell^2)_v = 4\beta$ at $\epsilon = -\epsilon_0$, where $k_-^2 = 0$, while equations (23) and (30) show that $-(\partial^2\epsilon/\partial\ell^2)_n$ at $\epsilon = \epsilon_0$, differs only by a factor of 0.93. Similar approximate equalities between corresponding quantities at positive and negative energies in the range $-\epsilon_0 \leqslant \epsilon \leqslant \epsilon_0$ are indicated in table 1, which may also be used to interpolate for the $\ell = 0$ energy levels and their local second derivatives. The tabulated quantities are

$$u_- = (3\pi/8\epsilon_0)(v+\tfrac{1}{2})$$
$$b_- = (\partial^2\epsilon/\partial\ell^2)_v/4\beta \tag{31}$$

at energy $-\epsilon$ and

$$u_+ = 2-(3\pi/8\epsilon_0)(v+\tfrac{1}{2})$$
$$-b_+ = -(\partial^2\epsilon/\partial\ell^2)_n/4\beta \tag{32}$$

at energy ϵ. Recall also that $\epsilon_0 = (1/16\beta)$. The divergence of $b_\pm$ as $\epsilon \to 0$ is of order $[(1-k^2)\ell n(1-k^2)]^{-1}$ as $k^2 \to 1$, while $(\partial\epsilon/\partial v)_\ell$ and $(\partial\epsilon/\partial n)_\ell$ tend to zero as $[\ell n(1-k_\pm^2)]^{-1}$ in the same limit. At energies above the range covered by table 1, the dominant energy dependence comes from the term $(2k_+^2-1)^{3/2}$, which implies that the $\ell = 0$ energies are given by

$$(\epsilon_v/\epsilon_0) = f(k_+)[(3\pi/8\epsilon_0)(v+\tfrac{1}{2})]^{4/3} - 1 \tag{33}$$

Table 1. Scaled quantum numbers, $U_\pm$, and second derivatives $B_\pm$, given by equations (31) and (32).

ϵ	u_-	u_+	b_-	b_+
0.00	1.0000	1.0000	∞	∞
0.05	0.9234	0.9237	11.2719	11.0934
0.10	0.8594	0.8607	6.2701	6.1144
0.15	0.8002	0.8028	4.4762	4.3349
0.20	0.7440	0.7481	3.5352	3.4045
0.25	0.6900	0.6960	2.9494	2.8271
0.30	0.6377	0.6458	2.5470	2.4317
0.35	0.5868	0.5972	2.2521	2.1427
0.40	0.5372	0.5501	2.0259	1.9217
0.45	0.4886	0.5041	1.8464	1.7467
0.50	0.4409	0.4593	1.7002	1.6045
0.55	0.3941	0.4154	1.5786	1.4866
0.60	0.3480	0.3723	1.4756	1.3869
0.65	0.3026	0.3301	1.3873	1.3016
0.70	0.2579	0.2886	1.3105	1.2277
0.75	0.2137	0.2478	1.2432	1.1629
0.80	0.1700	0.2076	1.1835	1.1056
0.85	0.1268	0.1679	1.1303	1.0546
0.90	0.0841	0.1289	1.0825	1.0089
0.95	0.0419	0.0903	1.0393	0.9676
1.00	0.0000	0.0522	1.0000	0.9302

where $f(k_+)$ varies from 1.217 at $k_+^2 = 0.85$ ($\epsilon \doteq \epsilon_0$) to 1.162 at $k^2 = 0.70$ ($\epsilon \doteq 5.25\ \epsilon_0$). Finally the second derivative $(\partial^2\epsilon/\partial\ell^2)_n$ continues to decrease monotonically to zero as $\epsilon \to \infty$ ($k_+^2 \to 0.5$).

The physical origin of the relative magnitudes and signs of the two final columns in table 1 may be understood by relating the second partial derivatives to angular velocities in the forms $(\partial^2 E/\partial\ell^2)_v = \ell^{-1}(\mathrm{d}\theta/\mathrm{d}t)$ for $\epsilon = \epsilon_- < 0$ and $(\partial^2 E/\partial\ell^2)_n = \ell^{-1}(\mathrm{d}\theta'/\mathrm{d}t)$ for $\epsilon = \epsilon_+ > 0$. Here θ is the polar angle and θ' is the angle conjugate to ℓ in the (n, ℓ) system—as discussed at the end of section 2; $\theta' = \theta - \frac{1}{2}\theta_R$ where θ_R is the angle conjugate to the radial action I_R. Estimates for these angular velocities may be obtained by comparing the vibrational time periods $T_\pm$ at energies $\epsilon_\pm$ respectively with corresponding angle changes, in the approximation that the latter are dominated by the torques at small r values, where a quadratic approximation to the potential is valid. The trajectory segments from one radial maximum to the next (see figure 1) then follow hyperbolic paths which may be parametrized for angular momentum ℓ and $\epsilon = \epsilon_-$ as $(x, y) = (\sqrt{2\epsilon_x}\cosh t, \sqrt{2\epsilon_y}\sinh t)$ where $2\epsilon_x = \sqrt{\epsilon_-^2 + \ell^2} - \epsilon_-$ and $2\epsilon_y = \sqrt{\epsilon_-^2 + \ell^2} + \epsilon_-$. The corresponding form for the ϵ_+ trajectory is $(x, y) = (-\sqrt{2\epsilon_x'}\sinh t, \sqrt{2\epsilon_y'}\cosh t)$, where $2\epsilon_x' = \sqrt{\epsilon_+^2 + \ell^2} + \epsilon_+$ and $2\epsilon_y' = \sqrt{\epsilon_+^2 + \ell^2} - \epsilon_+$. The convenience of this choice is that the final ($t \to \infty$) asymptote of the ϵ_- trajectory coincides with the initial ($t \to \infty$) asymptote of the ϵ_+ one, if $\epsilon_- = -\epsilon_+$. Hence, the two angle changes are related by $\Delta\theta_- + \Delta\theta_+ = \pi$. It also follows by simple trigonometry that $\Delta\theta_- = \arctan(\ell/\sqrt{\epsilon_-^2 + \ell^2})$. Moreover, the radial angle θ_R increases by 2π for each vibrational period. The final conclusion on taking the limit $\ell \to 0$ is that $(\partial^2 E/\partial\ell^2)_v \doteq |\epsilon T_-|^{-1}$ for $\epsilon < 0$, while $(\partial^2 E/\partial\ell^2)_n = |\epsilon T_+|^{-1}$ for $\epsilon > 0$. We also see

from table 1 that the time periods $T = 2\pi(\partial E/\partial v)_\ell^{-1}$ for the corresponding trajectories are quite similar.

4. The quantum-mechanical spectrum

The scaling in equation (17) reduces the quantum-mechanical Hamiltonian to the form

$$\hat{h} = -\frac{1}{2}\left[\frac{1}{r}\frac{\partial}{\partial r}\left(r\frac{\partial}{\partial r}\right) - \frac{\ell^2}{r^2}\right] - \frac{1}{2}r^2 + \beta r^4. \tag{34}$$

Numerically accurate eigenvalues are readily obtained by an expansion in normalized degenerate harmonic oscillator states

$$\psi(r) = \sum_n c_n \phi_{n\ell}(r) \tag{35}$$

where

$$\phi_{n\ell}(r) = \left[\frac{2\{(n-\ell)/2\}!}{\{(n+\ell)/2\}!}\right]^{\frac{1}{2}} r^\ell L^\ell_{(n-\ell)/2}(r^2) \tag{36}$$

in which L_v^α(z) is the associated Laguerre polynomial [8] and ℓ is taken to be positive. The necessary matrix elements follow from the recurrence relations

$$2\hat{t}\phi_{n,\ell} = \tfrac{1}{2}[(n+2)^2 - \ell^2]^{\frac{1}{2}}\phi_{n+2,\ell} + (n+1)\phi_{n,\ell} + \tfrac{1}{2}[n^2-\ell^2]^{\frac{1}{2}}\phi_{n-2,\ell} \tag{37}$$

$$r^2\phi_{n,\ell} = -\tfrac{1}{2}[(n+2)^2 - \ell^2]^{\frac{1}{2}}\phi_{n+2,\ell} + (n+1)\phi_{n,\ell} - \tfrac{1}{2}[n^2-\ell^2]^{\frac{1}{2}}\phi_{n-2,\ell} \tag{38}$$

where

$$\hat{t} = -\frac{1}{2}\left[\frac{1}{r}\frac{\partial}{\partial r}\left(r\frac{\partial}{\partial r}\right) - \frac{\ell^2}{r^2}\right]. \tag{39}$$

Terms in r^4 in equation (34) are obtained by repeating equation (38). Numerical convergence with respect to truncation of the resulting tridiagonal matrix naturally depends on the parameter β. The lowest 15 levels for $\beta = 0.005$, were converged to six decimal places after truncation of the sum in (35) to 50 terms.

The points in figure 3 mark the numerically determined eigenvalues around $\epsilon = 0$ for $-10 < \ell < 10$. Note that low-energy points with $0 \leqslant v \leqslant 3$ have been omitted and that the highest point at $L = 0$ corresponds to $v = 15$. To bring out the underlying patterns, full and broken lines are used to join points with a common radial quantum number, v, and a common 'total' quantum number, $n = 2v + |\ell|$, respectively. All the qualitative features predicted by the previous semiclassical arguments are clearly apparent. The v quantized curves show a sharp transition from smooth variation through $\ell = 0$ when $\epsilon < 0$, to a discontinuous first deriviative when $\epsilon > 0$, while the opposite is true for the broken n quantized curves. There is also a near symmetry between the positive $(\partial^2 E/\partial\ell^2)_v$ and the negative $(\partial^2 E/\partial\ell^2)_n$ second derivatives when the sign of the energy is reversed.

Quantitative comparison of the quantum-mechanical eigenvalues and their semiclassical counterparts derived from equation (18) reveals close agreement apart from a systematic discrepancy for levels around $\epsilon = 0$ and $\ell = 0$, of the form illustrated in figure 4. The points mark the discrepancies at the calculated quantum-mechanical energies for $\beta = 0.005$ and the curves indicate the form of a semiclassical correction function which is derived in the following section.

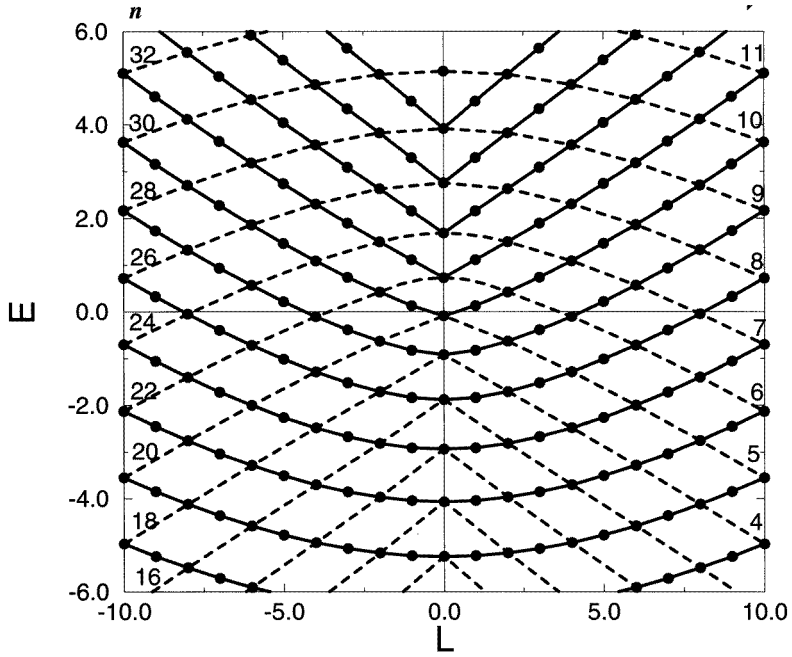

Figure 3. The central part of the quantum-mechanical spectrum equivalent to figure 2(*a*), organized according to the two quantization schemes. Full and broken lines join points with common v and common $n = 2v + |\ell|$ values respectively. The quantum numbers are given to the right and left respectively. Curves for odd n values, which join points with odd ℓ have been omitted for clarity.

5. Local corrections to the Bohr–Sommerfeld rule

The Bohr–Sommerfeld rule (18) follows directly from the form of the JWKB wavefunction on the assumption that the radial motion is bounded by two isolated turning points, each of which contributes a Maslov contribution of $\pi/4$ to the overall phase [1]. A correction to allow for coalescence of the inner turning point with the singularity in equation (4) at $r = 0$ may be obtained by comparison of the JWKB wavefunction with the asymptotic properties of solutions to a model equation with the same disposition of singularities and turning points near $r = 0$ [1, 13, 14].

The obvious form for the comparison is

$$\left[-\frac{1}{2}\frac{1}{r}\frac{\mathrm{d}}{\mathrm{d}r}\left(r\frac{\mathrm{d}}{\mathrm{d}r}\right) - \frac{\ell^2}{r^2} - \frac{1}{2}r^2\right]\Psi = \epsilon\Psi \tag{40}$$

which transforms under the substitutions, valid for $\ell > 0$,

$$z = r^2 \tag{41}$$

$$\Psi = z^{\ell/2}\Phi \tag{42}$$

to

$$\left(z\frac{\mathrm{d}^2}{\mathrm{d}z^2} + (\ell+1)\frac{\mathrm{d}}{\mathrm{d}z} + \frac{1}{4}z + \frac{\epsilon}{2}\right)\Phi = 0. \tag{43}$$

The further substitutions

$$z = \mathrm{i}\xi \tag{44}$$

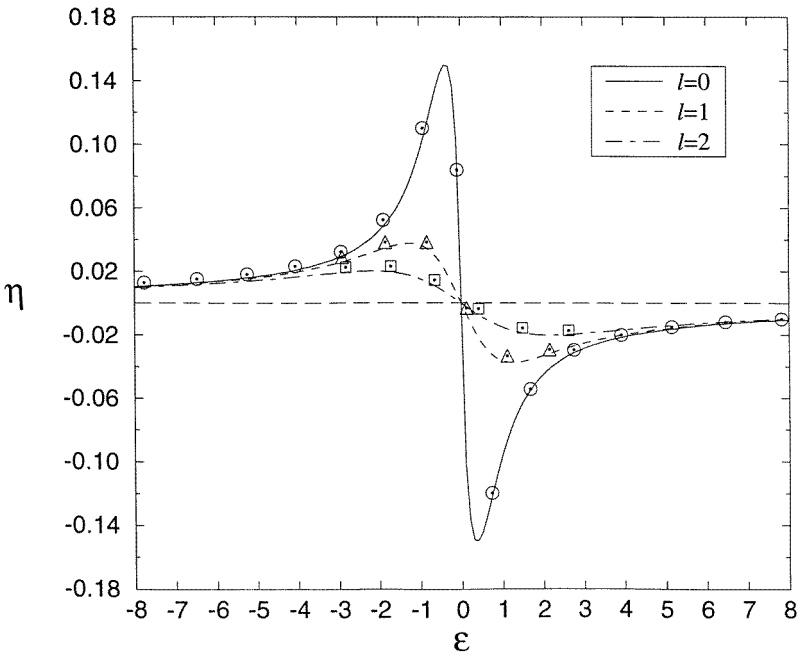

Figure 4. The semiclassical phase correction $\eta(\epsilon, \ell)$ functions for $\ell = 0, 1$ and 2. The points indicate discrepancies between the Bohr–Sommerfeld and quantum-mechanical eigenvalues in the form $\pi(\epsilon_{\text{Bohr}} - \epsilon_{\text{quantum}})/(\partial\epsilon/\partial v)_\ell$, suggested by equation (59).

$$\Phi = \mathrm{e}^{-\frac{1}{2}\xi}\chi \tag{45}$$

then lead to a form of Kummer's equation [8].

$$\left[\xi\frac{\mathrm{d}^2}{\mathrm{d}\xi^2} + (\ell + 1 - \xi)\frac{\mathrm{d}}{\mathrm{d}\xi} - \frac{1}{2}(\ell + 1 - \mathrm{i}\epsilon)\right]\chi = 0 \tag{46}$$

with the regular solution

$$\chi = M\left(\frac{\ell + 1 - \mathrm{i}\epsilon}{2}, \ell + 1, \xi\right) \tag{47}$$

where $M(a, b, \xi)$ is the confluent hypergeometric function [8]. It follows on combining (41), (42), (44), (45) and (47) that

$$\Psi = z^{\ell/2}\mathrm{e}^{-\mathrm{i}z/2}M\left(\frac{\ell + 1 - \mathrm{i}\epsilon}{2}, \ell + 1, \mathrm{i}z\right). \tag{48}$$

The asymptotic expansion [8] valid for $-\frac{\pi}{2} < \arg \mathrm{i}z < \frac{3\pi}{2}$

$$M(b + \mathrm{i}c, 2b, \mathrm{i}c) \sim \Gamma(b)[\mathrm{e}^{\mathrm{i}\pi(b+\mathrm{i}c)}(\mathrm{i}z)^{-b-\mathrm{i}c}/\Gamma(b - \mathrm{i}c) + \mathrm{e}^{\mathrm{i}z}(\mathrm{i}z)^{-b+\mathrm{i}c}/\Gamma(b + \mathrm{i}c)] \tag{49}$$

converts to the following asymptotic form for Ψ:

$$\Psi \sim Cz^{-\frac{1}{2}}\cos\left[\frac{z}{2} + \frac{\epsilon}{2}\ell nz - (\ell + 1)\frac{\pi}{4} - \arg\Gamma\left(\frac{\ell + 1 + \mathrm{i}\epsilon}{2}\right)\right] \tag{50}$$

where C is an unimportant normalizing factor.

Turning to the JWKB function, the substitution

$$r = \mathrm{e}^x \tag{51}$$

casts equation (40) into the form

$$\left[\frac{\mathrm{d}^2}{\mathrm{d}x^2} + k_\ell^2(x)\right]\Psi = 0 \tag{52}$$

where

$$k_\ell^2(x) = 2\epsilon \mathrm{e}^{2x} - \ell^2 + \mathrm{e}^{4x}. \tag{53}$$

The substitution $z = \mathrm{e}^{2x}$ therefore leads to the following form for the JWKB phase [1, 14]

$$\begin{aligned}\int_{x_1}^{x} k_\ell(x)\,\mathrm{d}x &= \frac{1}{2}\int_{z_1}^{z} \frac{\sqrt{z^2+2\epsilon z-\ell^2}}{z}\,\mathrm{d}z = \Bigg[(z^2+2\epsilon z-\ell^2)^{\frac{1}{2}} \\ &\quad -\ell \arctan\left(\frac{\epsilon z-\ell}{\ell(z^2+2\epsilon z-\ell^2)^{\frac{1}{2}}}\right) + \epsilon \ln(2(z^2+2\epsilon z-\ell^2)^{\frac{1}{2}}+2z+2\epsilon)\Bigg]_{z_1}^{z} \\ &\sim \frac{1}{2}z + \frac{\epsilon}{2}\ln z + \frac{\epsilon}{2} - \frac{\ell}{2}\arctan\left(\frac{\epsilon}{\ell}\right) - \frac{\epsilon}{4}\ln\left(\frac{\epsilon^2+\ell^2}{4}\right)\frac{-\ell\pi}{4}.\end{aligned} \tag{54}$$

It follows that the argument of

$$\Psi_{\mathrm{JWKB}} \sim C z^{-\frac{1}{2}} \cos\left(\frac{1}{2}\int_{z_1}^{z} \frac{(z^2+2\epsilon z-\ell^2)^{\frac{1}{2}}}{z}\,\mathrm{d}z - \frac{\pi}{4}\right) \tag{55}$$

differs from that in (50) by a term

$$\eta(\epsilon,\ell) = \frac{\epsilon}{4}\ln\left(\frac{\epsilon^2+\ell^2}{4}\right) - \frac{\epsilon}{2} + \frac{\ell}{2}\arctan\left(\frac{\epsilon}{\ell}\right) - \arg\Gamma\left(\frac{|\ell|+1}{2} + \frac{\mathrm{i}\epsilon}{2}\right) \tag{56}$$

which corrects for neglect of the singular behaviour at $z = 0$ in the primitive JWKB approximation. To avoid ambiguity, ℓ in the argument of the Γ function has been replaced by $|\ell|$ because the regular form for Ψ in (42) would require the substitution of $-\ell$ for ℓ in equations (42)–(50) if ℓ were negative. The improved quantization formula is obtained by adding this correction to equation (18); thus

$$\frac{1}{2}\int_{z_1}^{z_2} \frac{\left(z^2+2\epsilon z-2\beta z^3-\ell^2\right)^{\frac{1}{2}}}{z}\,\mathrm{d}z + \eta(\epsilon,\ell) = \left(v+\frac{1}{2}\right)\pi. \tag{57}$$

Its local nature may be seen by using Stirling's approximation [8] to evaluate $\Gamma\left(\frac{\ell+1+\mathrm{i}\epsilon}{2}\right)$, with the result for large $\left|\frac{\ell+1+\mathrm{i}\epsilon}{2}\right|$

$$\eta(\epsilon,\ell) \sim -\frac{1}{2}\frac{\epsilon}{(\ell+1)^2+\epsilon^2}. \tag{58}$$

The introduction of this phase correction in equation (57) translates into a correction to the energy of order

$$\begin{aligned}\Delta\epsilon &= (\epsilon - \epsilon_{\mathrm{JWKB}}) \\ &= -(\eta(\epsilon,\ell)/\pi)(\partial\epsilon/\partial v)_\ell\end{aligned} \tag{59}$$

where $(\partial\epsilon/\partial v)_\ell$ is the local energy separation, because v changes by one unit from one energy to the next. Figure 4 confirms that this correction accounts almost entirely for the error in the Bohr–Sommerfeld energy levels, in the given test case $\beta = 0.005$. It is seen that $\eta(\epsilon,\ell) = -\eta(-\epsilon,\ell)$, with a maximum magnitude of 0.15 at $|\epsilon| = 0.356$, which translates, via equation (59), to a maximum error in ϵ_{JWKE} of only 5% of the local energy separation.

6. Summary and conclusions

Features of the quantum-mechanical eigenvalue spectrum of degenerate double minimum champagne bottle have been related to the following aspects of the underlying classical mechanics.

(a) The known [2] absence of a global system of angle-action variables is reflected in a sharp change in the energy level pattern organized by a radial quantum number v and angular mementum ℓ. The levels vary smoothly with ℓ at constant v for $\epsilon < 0$, but there is sharp discontinuity in the derivative $(\partial\epsilon/\partial\ell)_v$ at $\ell = 0$ for $\epsilon > 0$.

(b) An alternative (n, ℓ) quantization scheme, where $n = 2v + |\ell|$, shows the opposite effect. The derivative $(\partial\epsilon/\partial\ell)_n$ is continuous for $\epsilon > 0$ but has a discontinuity at $\ell = 0$ for $\epsilon < 0$.

(c) A near symmetry between positive and negative second derivatives $(\partial^2\epsilon/\partial\ell^2)_v$ for $\epsilon < 0$ and $(\partial^2\epsilon/\partial\ell^2)_n$ for $\epsilon > 0$, over the range $-\epsilon_0 < \epsilon < \epsilon_0$, where ϵ_0 is the well depth, was related to the near hyperbolic nature of two different types of trajectory segments at corresponding positive and negative energies. Similar near symmetries in the vibrational level densities and the number of bound levels in the energy ranges $-\epsilon_0 < \epsilon < 0$ and $0 < \epsilon < \epsilon_0$ were also identified.

(d) The main conclusions, including a formula $v_0 + \frac{1}{2} = (8\epsilon_0/3\pi)$ for the number of $\ell = 0$ states with $\epsilon < 0$, were deduced at the Bohr–Sommerfeld level. A comparison with numerically accurate quantum-mechanical eigenvalues revealed a systematic discrepancy for levels with $\epsilon \doteq 0$ and $\ell \doteq 0$, which were removed by incorporation of an analytical phase correction $\eta(\epsilon, \ell)$ to the usual semiclassical Maslov term.

Acknowledgments

Professor R Cushman is gratefully acknowledged for drawing attention to this interesting system. Thanks are given to the UK EPSRC for organizing a workshop at the University of Warwick, where the discussions took place.

References

[1] Child M S 1991 *Semiclassical Mechanics with Molecular Applications* (Oxford: Oxford University Press)
[2] Bates L M 1991 *J. Appl. Math. Phys.* **42** 837
[3] Duistermaat J J 1980 *Commun. Pure Appl. Math.* **33** 687
[4] Cushman R and Duistermaat J J 1988 *Bull. Am. Math. Soc.* **19** 475
[5] Cushman R and Knörrer H 1981 *Lecture Notes in Maths* vol 1139 (New York: Springer) p 12
[6] van der Meer J C 1985 *Lecture Notes in Maths* vol 1160 (New York: Springer)
[7] Carter S and Sutcliffe B T 1982 *Mol. Phys.* **47** 1445
[8] Abramowitz M and Stegun I A 1965 *Handbook of Mathematical Functions* (New York: Dover)
[9] Born M 1960 *Mechanics of the Atom* (London: Bell and Sons)
[10] Gradsteyn I S and Ryzhik I M 1965 *Tables of Integrals, Series and Products* (New York: Academic)
[11] Gröbner W and Hofreister N 1966 *Integraltafeln* vol I (Vienna: Springer)
Gröbner W and Hofreister N 1966 *Integraltafeln* vol II (Vienna: Springer)
[12] Goldstein H 1959 *Classical Mechanics* (New York: Addison-Wesley)
[13] Langer R E 1937 *Phys. Rev.* **51** 669
[14] Froman N and Froman P O 1967 *JWKB Approximation, Contributions to the Theory* (Amsterdam: North-Holland)